Stem Cell Reviews and Reports (2022) 18:1025–1040
https://doi.org/10.1007/s12015-021-10176-0

Extracellular Vesicles from Human Umbilical Cord Mesenchymal Stem Cells Facilitate Diabetic Wound Healing Through MiR-17-5p-mediated Enhancement of Angiogenesis

Qian Wei[1,2] · Yaxi Wang[1,2] · Kui Ma[1,3,4] · Qiankun Li[1] · Bingmin Li[1] · Wenzhi Hu[1] · Xiaobing Fu[1,2,3,4] · Cuiping Zhang[1,3,4]

Accepted: 26 April 2021 / Published online: 4 May 2021

Abstract

Endothelial dysfunction caused by persistent hyperglycemia in diabetes is responsible for impaired angiogenesis in diabetic wounds. Extracellular vehicles (EVs) are considered potential therapeutic tools to promote diabetic wound healing. The aim of this study was to investigate the effects of EVs secreted by human umbilical cord mesenchymal stem cells (hucMSC-EVs) on angiogenesis under high glucose (HG) conditions *in vivo* and *in vitro* and to explore the underlying mechanisms. *In vivo*, local application of hucMSC-EVs enhanced wound healing and angiogenesis. *In vitro*, hucMSC-EVs promoted proliferation, migration, and tube formation by inhibiting phosphatase and tensin homolog (PTEN) expression and activating the AKT/HIF-1α/VEGF pathways. MiR-17-5p was found to be highly enriched in hucMSC-EVs. *In vitro*, MiR-17-5p agomirs downregulated the expression of PTEN and activated the AKT/HIF-1α/VEGF pathway to promote proliferation, migration, and tube formation in HG-treated HUVECs. *In vivo*, miR-17-5p agomirs mimicked the effects of hucMSC-EVs on wound healing and angiogenesis, whereas miR-17-5p inhibitors reversed their effects. Our findings suggest that hucMSC-EVs have regenerative and protective effects on HG-induced endothelial cells via transfer of miR-17-5p targeting PTEN/ AKT/HIF-1α/VEGF pathway, thereby accelerating diabetic wound healing. Thus, hucMSC-EVs may be promising therapeutic candidates for improving diabetic wound angiogenesis.

Keywords Diabetic wounds · Mesenchymal stem cells · Extracellular vesicles · miR-17-5p/PTEN/AKT/HIF-1α/VEGF pathway · Angiogenesis

Introduction

Diabetes is a multifaceted metabolic disorder. Nearly 20 % of diabetics worldwide develop prolonged wounds, which may lead to the formation of skin ulceration [1]. In China, diabetes has also become the major culprit of chronic skin wounds in hospitalized patients. The prevalence increased from 4.91 % to 1996 to 35.3 % in 2008, which burdened both individuals and the health care resources[2, 3]. According to statistic, the average duration of hospitalization was 31 days with a medical cost of ¥17,181.9[3]. Leg and foot ulcers are the most common types of diabetic wounds. Diabetic foot ulceration results in amputation in 15–27 % of patients if not properly diagnosed and treated [4]. Despite improvements in wound repair, cure of chronic diabetic wounds remains a distant goal because of impaired healing. Angiogenesis plays a critical role in the wound healing process, facilitating the transport of nutrients and oxygen to lesion sites and enhancing fibroblasts multiplication, collagen synthesis and re-epithelization [5, 6]. Hypo-vascularization is associated with

✉ Xiaobing Fu
fuxiaobing@vip.sina.com

✉ Cuiping Zhang
zcp666666@sohu.com

1 Research Center for Tissue Repair and Regeneration Affiliated to the Medical Innovation Research Division and 4th Medical Center of Chinese PLA General Hospital, 51 Fucheng Road, Haidian District, Beijing 100048, China

2 Chinese PLA Medical School, 28 Fuxing Road, Haidian District, 100853 Beijing, China

3 Research Unit of Trauma Care, Tissue Repair and Regeneration, Chinese Academy of Medical Sciences, 2019RU051, 51 Fucheng Road, Haidian District, 100048 Beijing, China

4 Beijing Key Research Laboratory of Skin Injury, Repair and Regeneration, 51 Fucheng Road, Haidian District, 100048 Beijing, China

delayed or dysfunctional healing of diabetic wounds [7, 8]. Furthermore, hyperglycemia, a typical characteristic of diabetes, is commonly associated with refractory wounds and endothelial malfunction, leading to vascular complications such as diabetic foot ulceration [9]. Accordingly, novel remedies to promote angiogenesis would be highly valuable for managing diabetic wounds.

Mesenchymal stem cells (MSCs) have been shown to promote angiogenesis in ischemic conditions such as chronic wounds [10–12], myocardial infarction [13, 14], and cerebral ischemia [15, 16]. For example, human umbilical cord MSCs (hucMSCs) relieved hind limb ischemia by promoting angiogenesis in mice [17]. Recently, promotion of angiogenesis by MSCs has increasingly been attributed to exocrine factors [18, 19]. EVs carry molecules including proteins, mRNAs, and miRNAs, and have been demonstrated to act as paracrine factors to regulate the interactions between MSCs and target cells. Compared with their parental MSCs, EVs have several advantages including high stability, increased therapeutic efficiency and safety, absence of immune reactions, fewer ethical issues, and decreased potential in embolism formation and carcinogenicity [20–23]. EVs derived from many sources of MSCs have been reported to promote angiogenesis and represent promising treatment options for diabetic wounds. For instance, EVs derived from hucMSCs (hucMSC-EVs) and lipopolysaccharide-preconditioned hucMSC-EVs regulated macrophage plasticity to resolve chronic inflammation during diabetic wound healing [24]. However, whether hucMSC-EVs can restore the proangiogenic ability of endothelial cells injured under high glucose (HG) conditions remains to be confirmed.

EVs contain multiple types of information-containing molecules including miRNAs, non-coding small RNAs that can bind to the 3′- untranslated region of mRNAs to inhibit target gene's expression. MiRNAs in EVs have important regulatory functions and may participate in wound healing and angiogenesis. For example, EVs derived from human adipose-derived MSCs transferred miRNA-125a to endothelial cells and promoted angiogenesis *in vivo* and *in vitro* by repressing Delta-like 4 expression [25]. Circulating EVs containing miR-20b-5p isolated from diabetic patients slowed wound healing and angiogenesis by targeting Wnt9b/β-catenin signaling [26]. Recently, hucMSC-EVs combined with pluronic F127 hydrogel were reported to have beneficial effects for diabetic wound treatment [27], but the mechanisms through which hucMSC-EVs exert their functions remain unclear.

In this study, we first assessed the effects of hucMSC-EVs on diabetic wound healing and angiogenesis. We used hucMSC-EVs to treat human umbilical vascular endothelial cells (HUVECs) exposed to HG. Subsequently, the proliferation, migration, tube formation, and senescence of HUVECs were examined. Expression of angiogenesis-related proteins including phosphatase and tensin homolog (PTEN), p-AKT, hypoxia inducible factor (HIF)-1α, and vascular endothelial growth factor (VEGF) was assessed. We also identified candidate miRNAs in hucMSC-EVs and showed that these could improve endothelial cell function and target the PTEN/AKT/HIF-1α/VEGF pathways.

Methods

Culture and Identification of HucMSCs

The hucMSCs (P1) were acquired from the Chinese Academy of Sciences' cell bank and cultured in Dulbecco's modified Eagle's medium/F12 (DMEM/F12, Gibco, USA), containing 10 % Fetal Bovine Serum (Gibco, USA) and 1 % penicillin and streptomycin (Gibco, USA). The flow cytometer was employed to determine cell surface markers of hucMSCs. The hucMSCs were washed and co-incubated with fluorescence-conjugated antibodies (Abcam, USA) (CD73-PE, CD90-FITC, CD105-FITC, CD45-FITC, CD19-FITC, HLA-DR-FITC and CD34FITC) at room temperature for three quarters of an hour. To identify the multi-differentiation potential, hucMSCs were incubated with chondrogenic, adipogenic and osteogenic differentiation medium (Cyagen, China), respectively. Next, these induced cells were stained severally with Alcian blue, Oil Red O, and Alizarin Red S to evaluate chondrogenic, adipogenic, and osteogenic differentiation. Then these cell images were filmed with an Olympus IX71 light microscope (Olympus, Japan).

Isolation and Characteristics of HucMSC-EVs

After 2–3 passages, the culture medium of hucMSCs was changed into DMEM/F12 containing 10 % EV-free FBS (SBI, USA). Besides, all hucMSCs were from at least four people, and the supernatants of these cells from passage 3 to passage 7 were mixed together. The cultured supernatants of hucMSCs were collected every 72 h starting from passage 3 until passage 7. EVs were harvested from supernatant by means of a series of ultra-high-speed centrifugation procedures according to the protocol illustrated by Jia et al. [28]. Supernatants of cell cultures were collected and centrifuged at 2,000 x g for 10 min at 4 to remove dead cells, cellular debris and apoptotic bodies. Next, the supernatants were centrifuged at 10,000 x g for 30 min at 4 °C. We collected the supernatants and ultracentrifuged them at 100,000 x g for 75 min at 4 °C. Then the supernatants were discarded, the deposition was re-suspended with 1ml PBS and submitted to a 0.22 μm sterile filter. Supernatants were ultracentrifuged at 100,000 x g for 75 min at 4 °C again. We discarded the supernatants and resuspended the EVs with PBS for following use or store at -80 °C. About 5×10^8 cells will produce 8.77×10^9 EV particles or 710 μg EVs. The characteristics of hucMSC-EVs were

conducted by nanoparticle tracking analyzer (NTA) (Particle Metrix GmbH, Germany) and transmission electron microscope (TEM) (Hitachi, Japan). Expressions of the hucMSC-EVs markers, containing CD63, CD9 and the tumor susceptibility gene101 (TSG101), were examined by Western blot.

In Vivo Administration of HucMSC-EVs

All animal procedures involved were approved by the Animal Research Committee of PLA General Hospital in Beijing, China and were conducted in accordance with the principles and procedures of the National Institutes of Health (NIH) Guide for the Care and Use of Laboratory Animals. Remarkable efforts were made to minimize the number of animals and their sufferings. We have selected male diabetic mice of 8 weeks (BKS-Dock Lepr^{em2Cd479}, db/db), and db/db mouse is a widely used type II diabetic mouse model that displays many of the characteristics of the human disease including hyperglycemia, insulin resistance, and obesity [29]. These mice are already markedly obese with substantial fasting hyperglycemia (Figure S1). They weighed about 35 g, were anesthetized with 4 % chloral hydrate. Full-thickness skin wounds of 10mm in diameter were created on the backs of diabetic mice. Afterward, all mice were randomly divided into EV groups (4, 8, and 12 days) and control groups (4, 8, and 12 days). There were five mice for each time point. HucMSC-EVs (50μL, 2.25×10^9 particles/mL)1 and PBS (50 μL) were injected around the wounds at 4 sites (12.5 μL per site) with a micro syringe (Hamilton) at every other day, and hucMSC-EV concentration was selected based on the results of the preliminary experiment (Figure S2). Moreover, during the experiment, all mice were kept in SPF facility, provided with SPF water, SPF food and clean bedding. They were checked once a day. The weight of mice in each group increased gradually and the difference was not statistically significant (Figure S1 A, $P > 0.3$). There was no significant difference between two groups in terms of blood glucose before, during and post wound healing (Figure S1 B, $P > 0.05$).

Wound Closure Evaluation and Neovascularization Observation

Wounds from each group were imaged at 0, 4, 8, and 12 day post-wounding. All wounds were calculated with a caliper ruler and areas of them were evaluated in Image -Pro Plus software (Media Cybernetics, USA). The wound closing rate was calculated as the following formula: $(A_0 - A_t) / A_0 \times 100\ \%$. A_0 represented the primary wound area and A_t represented the wound area at 4, 8, and 12 days. To detect the generation of new blood vessels, the skin underside at day 12 was observed and captured using a stereomicroscope (Leica Germany) at 10 × magnification. The percentage of neovessels in the detected field was calculated via ImageJ. We changed the images into 8 binary digit forms, inverted them, adjusted the threshold to outline vessel areas. Then the vessel areas were measured.

Histological Analysis and Immunohistochemistry

After the mice were put to euthanasia by being excessively injected with pentobarbital, wound sites were obtained and fixed postoperatively. The obtained tissues were dehydrated step and step and embedded in paraffin. Subsequently, these embedded tissues were cut into 5 μm thick sections and stained with hematoxylin and eosin (H&E). Measurement of scar width and neo-epithelium percentage was performed as previously described [30]. Masson's trichrome was stained to assess the extent of collagen maturity. Collagen volume fraction were quantified according to literature previously described [31].

Immunohistochemistry staining for CD31 (Abcam, the USA, ab28364, 1:100) was conducted to examine the degree of newly-formed capillaries in wound sites. Briefly, the paraffin sections were incubated with the primary CD31 antibody overnight at 4 °C and then with the secondary HRP-conjugated antibody (1:200, Abcam) for 1 h at room temperature. Finally, the sections were colored by a DAB kit (ZSGB-BIO, China). Images were photographed under a microscope and measured as literature previously described [32].

Blood Perfusion Evaluation

On day 12 post operation, we applied laser speckle contrast imaging (LSCI) to investigate the wound perfusion. A PeriCam PSI-ZR (PERIMED Ltd, Sweden) was employed to record images of each wound. A unit of perfusion was detected based on a near-infrared laser (785 nm) for perfusion measurements. Images were captured using the same scan site dimensions at a fixed distance from the wound surface. Applying PIMSoft (Moor Instruments Ltd, UK), flux photographs of each wound were estimated to evaluate the mean perfusion units (MPUs) ratio calculated by comparing the MPUs at the wound site (ROI-1) with that of the area besides the wound (ROI-2).

Cell Culture and HucMSC-EVs Uptake

HUVECs were obtained from the Chinese Academy of Sciences (Shanghai, China). These cells were incubated in Dulbecco's modified Eagle's medium (DMEM, Gibco, USA) consisting of 10 % fetal bovine serum (Gibco, USA) and 1 % penicillinstreptomycin. The normal glucose (NG) concentration is 5.5 mM. To examine hucMSC-EVs uptake by HUVECs, EVs were labeled with PKH67 (Sigma-Aldrich, Germany), a green fluorescent dye, in the light of the manufacturer's protocol. Then, HUVECs were co-cultured with

PKH67-labeled EVs for 4.5 h and next fixed in 4 % paraformaldehyde for 15 min. After these cells were washed by PBS, HUVECs were incubated with CD31 antibody (1:100) overnight at 4 °C. Next Cy3-conjugated secondary antibody (Abcam, 1:500) and DPAI (Sigma-Aldrich, 2 mg/mL) were applied for the incubation for visualization. At last, HUVECs were observed via a confocal microscope (Leica, Germany).

Proliferation and Cell Cycle assay

For proliferation assay, HUVECs (8×10^3 cells per well) were seeded into 96-well plates. The cells in control group were cultured in NG concentration and those in HG group were incubated with 35 mM glucose for 7–9 days, mimicking the diabetic hyperglycemia in vivo[33]. Different concentrations of EVs (6.15×10^8, 1.23×10^9, 1.84×10^9, 2.04×10^9, 2.25×10^9 and 2.45×10^9 particles /mL) were added to the culture medium of HG-induced HUVECs to select the optimal concentration. On day 1, 3, 5 and 7, cell counting kit-8 (CCK-8, 10 μL per well, Dojindo Molecular Technologies, Japan) was added to the medium (100 μL per well). The absorbance of per well was examined at 450nm by an enzyme immunoassay analyzer (Bio-Rad 680, Hercules, USA) after incubation for 3 h at 37 °C. According to the results of CCK-8 assay, the optimal concentration of EVs, which had the most obvious effect on cell viability, was chosen to applied in the following experiments including cell cycle, cell migration, tube formation, and cellular senescence assays. Additionally, the expression of PTEN, p-AKT, AKT, HIF-1α, and VEGF was evaluated by Western blot.

For cell cycle assay, HUVECs (8×10^5 cells per well) were seeded in six-well plates and cultured in NG, HG and HG + EVs. After being cultured for 3 days, the cells were harvested from six-well plates and fixed with 70 % cold ethanol overnight at 4 °C. On the second day, single cell suspensions were put into digestion with 100 μl/well DNase-free RNase in incubator at 37 °C, and subsequently 400 μl of propidium iodide (PI) solution was added for DNA staining for 1 h at 4 °C. PI fluorescence as well as forward light scattering was examined with a flow cytometer (BD FACS Calibur™, Becton-Dickinson, USA). The percent of cells in different phases was calculated.

Cell Migration Assay

The migration property of HUVECs was evaluated by means of scratch and transwell assay. For scratch assay, HUVECs were cultured in six-well plates. When 90 % confluence was reached, cells were scratched with a pipette tip. At planned time point, cells were photographed using a microscope. Distances between two borders of the scratch were calculated by ImageJ software. The migration rate (%) was calculated as: $(M_0 - M_t) / M_0 \times 100$ %, in which M_0 stood for the initial scratch distances, while Mt represented the resting scratch distances at the surveyed time point. For transwell assay, approximate 0.5×10^4 HUVECs were suspended in serum-free medium and seeded into the upper chamber of 24-well plates (Corning) with 8.0 μm polycarbonate membrane. Then the complete medium (containing serum) supplemented with HG or EVs was added into the lower chamber. After 24 h, we swabbed the cells on the upper surface of the filter membranes and the migrated cells on the lower surface were stained with crystal violet (Solarbio, 0.1 %, w/v) for 7 min. The stained cells were observed and calculated under an optical microscope.

Tube Formation Assay

50 μl cold Matrigel was added into each well of a pre-cooling 96-well plate and next incubated at 37 for 30 min. HUVECs (2×10^4 cells per well, five replicates per group) were put into the Matrigel-coated plates and treated with different mediums (NG, HG and HG + EVs). After incubation for 6 h at 37 , tube formation was examined under a microscope. The parameters (total branching points and total tube length) demonstrating the tube formation capability were measured with Image-Pro Plus 6.0 software.

Detection of MiRNAs in HucMSC-EVs

MiRNA microarray and qRT-PCR were perform to find the candidate miRNAs in EVs which play an important role in hucMSC-EVs-induced effects. MiRNAs in EVs were isolated via the use of the SeraMir Exosome RNA Purification Kit (System Biosciences, Mountain View, USA). MiRNA microarray was conducted using GeneChip miRNA 4.0 array which contains 30,424 probe sets covering 2578 human miRNAs, 728 rat miRNAs, and 1908 mouse miRNAs. We selected the candidate miRNA according to the intensity of fluorescent signal of microarray. Based on the results of microarray, the higher the intensity value is, the more portion the miRNA accounts for (Figure S3). And our results demonstrated that miR-17-5p is the most abundant miRNA in EVs. The miRNA highly expressed in hucMSC-EVs were further confirmed by qRT-PCR. Bioinformatics analysis was conducted by programs including Targetscan (http://www.targetscan.org/), miRanda (http://www.microrna.org), and Pictar (http://pictar.mdc-berlin.de/). According to the results of miRNA detection and bioinformatics analysis, miR-17-5p was found to be the most highly expressed miRNA and target PTEN. Next, the potential role of miR-17-5p in hucMSC-EVs was explored.

MiRNA Interference

We obtained miR-17-5p inhibitors, negative control (NC) inhibitors, miR-17-5p agomirs, and negative control

agomirs from GenePharma (Suzhou, China). To produce EVs without miR-17-5p, miR-17-5p inhibitors or NC inhibitors (100 nmol/L) were transfected into hucMSCs which have grown to 80 % confluence with aid of Lipofectamine 2000 (Invitrogen, NY, USA). After 6 h, the transfected cells were maintained in the medium containing EVs-free FBS for 48 h. EVs were isolated from the conditioned medium of the cells transfected with miR-17-5p inhibitor or NC inhibitor. These EVs were named as EVs-inhibitor $^{miR-17-5p}$ (EVs without miR-17-5p) and EVs-inhibitor^{NC}, respectively. Next, HG-treated HUVECs were incubated with EVs-inhibitor $^{miR-17-5p}$ or EVs-inhibitor^{NC}, or transfected with miR-17-5p agomirs or NC agomirs. MiR-17-5p inhibitors were labeled by 5-Carboxyfluorescein (5-FAM, green) while miR-17-5p agomirs by Cyanine 3 dyes (Cy3, red). The transfection efficiency was evaluated by flow cytometry assay. The expressions of miR-17-5p and PTEN in HUVECs from different groups were detected by qRT-PCR. We also observed the expressions of PTEN, p-AKT, AKT, HIF-1α, and VEGF by Western blot. The proliferation, migration and tube formation abilities were investigated by the methods described above. Additionally, animal experiment with mice was also performed to evaluate the potential role of miR-17-5p in hucMSC-EVs. The experiment designs the groups as in the cellular experiments. Wound closure, blood perfusion and angiogenesis were examined by the methods in above animal experiment.

Western Blot

The total protein was extracted using RIPA buffer containing a protease phosphatase inhibitor mixture (Solarbio, China). The protein concentration was determined via the BCA method. 20 μg of protein extract was loaded in each lane (10 % SDS-PAGE) and electrotransferred onto PVDF membranes (Millipore). Next, the PVDF membranes were incubated with 5 % skimmed milk for 1 h and primary antibodies including anti-CD63, anti-TSG101, anti-CD9, anti-Calnexin, anti-AKT, anti-phosphorylate AKT (anti-p-AKT), anti-PTEN, anti-HIF1α, and anti-VEGF (1:1000, Abcam, USA) at 4 °C overnight. After being washed on the next day, these membranes were incubated with horseradish peroxidase-conjugated (HRP)-linked secondary antibodies (1:3000, ZSGB-BIO, China) for 1 h at room temperature. The immunoreactive bands were visualized via an ECL kit (Solarbio, China) and imaged by UVITEC Alliance MINI HD9 system (UVITEC, Britain). β-actin was used as an internal control. The gray value assay representing the protein expression level was quantified by ImageJ.

qRT-PCR Analysis

Total RNAs were extracted from HUVECs with Trizol Reagent (Invitrogen, USA). The mRNA was reverse transcribed using the Revert Aid first-strand cDNA synthesis kit (Fermentas, Life Sciences, Canada) and qPCR was conducted using FastStart Universal SYBR Green Master Mix (Roche, Indianapolis, USA) with ABI 7500 Real-Time PCR system. For detection of miRNAs, miRNAs in EVs were isolated via the use of the SeraMir Exosome RNA Purification Kit (System Biosciences, Mountain View, USA) and cDNA for miRNAs was integrated with TaqMan microRNA assay kit (Applied Biosystems, Foster City, USA) according to the manufacturer's protocol. qRT-PCR was conducted with an ABI PRISM®7900HT System with SYBR Premix ExTaqTM II (Takara Biotechnology, Japan). Stem-loop qRT-PCR for miRNA detection was employed. Data were collected and the relative expression levels were calculated by applying the $2^{-\Delta\Delta CT}$ method. Results were normalized to β-actin (for cellular PTEN mRNA) or U6 small nuclear RNA (for miRNAs in cells or EVs). The mRNA primers and the miRNA-specific forward primers were synthesized by Sangon Biotech (Shanghai, Table S1).

Statistical Analysis

All data were reported as mean ± standard deviation and evaluated with analysis of variance (ANOVA) and Student t test where appropriate. All experiments were carried out at least three times. Differences were considered to be statistically significant when $p < 0.05$.

Results

HucMSC-EVs Enhance Cutaneous Wound Healing in Diabetic Mice

HucMSCs were cultured and identified based on their morphology, phenotype, and function (Figure S4). EVs were isolated from hucMSCs and characterized by NTA, TEM and western blotting. NTA showed that the sizes of hucMSC-EVs ranged from 60 nm to 180 nm (mean diameter 100 nm), whereas the concentration of EVs was 8.77×10^9 particles/mL (Fig. 1a). TEM revealed that hucMSC-EVs had a "saucer-like" ultrastructure (Fig. 1b). Representative markers of EVs including TSG101, CD63 and CD9 were expressed by the hucMSC-EVs while expression of calnexin wasn't detected (Fig. 1c). These results, which were consistent with those of previous reports [34–36], demonstrated that the isolated nanoparticles were indeed EVs.

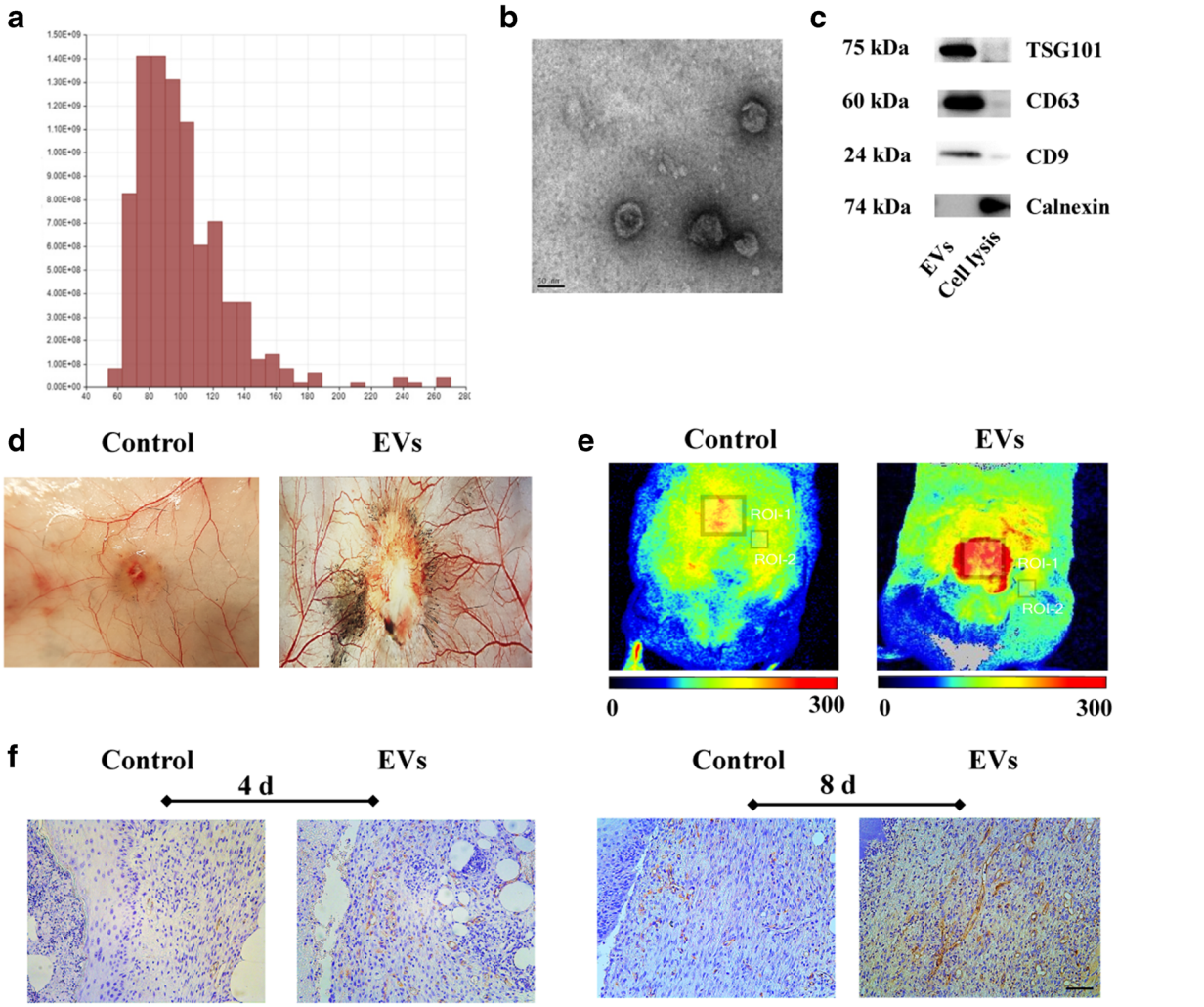

Fig. 1 Characteristics of hucMSC-EVs and improvement of diabetic wound healing and angiogenesis by hucMSC-EVs. **a** Particle size distribution and concentration results of hucMSC-EVs measured by qNano analysis. **b** TEM photomicrographs of hucMSC-EVs. Scale bar: 50 nm. **c** Western blot of EV markers in hucMSC-EVs. **d** Gross view of wounds from two groups at day 12 post wounding. Newly-formed blood vessels were found in the wound sections. **e** The blood flows at the wound sections from two groups were evaluated by doppler of animals, flux images of the wounds. **f** CD31 staining of wound sites in the control and hucMSC-EVs treated groups. Scale bar: 200 μm

To evaluate the effects of hucMSC-EVs on diabetic wound healing, we created full-thickness cutaneous wounds on the backs of diabetic mice and injected hucMSC-EVs or phosphate-buffered saline (PBS) around the wounds. Digital photographs of the wound sites taken at day 0, 4, 8, and 12 showed the progress of wound closure in different groups of mice. Gross observations showed that the hucMSC-EV-treated mice had reduced wound areas at days 4, 8, and 12 compared with PBS-treated control mice (Figure S5). The wounds of hucMSC-EV-treated mice had mostly recovered at day 12, whereas scar areas remained discernable in the control mice. The dimensions of the wound areas were measured 0, 4, 8, and 12 days after wounding. As shown in Figure S5, the extent of wound healing in hucMSC-EV-treated mice was significantly greater after 4, 8, and 12 days than that in control mice ($p < 0.001$). At 12 days after wounding, wounds in hucMSC-EV-treated mice were completely healed, whereas those of control mice still had approximately 40 % of their area remaining to be closed. Rapid reepithelialization is one of the key steps in wound healing. Consistent with the wound area observations, hematoxylin and eosin staining showed that hucMSC-EV-treated wounds had longer neo-epidermis and dermis lengths than those of PBS-treated wounds at day 4, 8, and 12 post-wounding (Figure S6). Masson staining also revealed a greater number of wavy fibers in EV-treated wounds compared with control wounds (Figure S7). These data suggested that hucMSC-EVs treatment can promote wound healing in diabetic mice.

HucMSC-EVs Promote Angiogenesis in the Wound Sites of Diabetic Mice

We next assessed whether treatment with hucMSC-EVs could promote angiogenesis at wound sites, thereby enhancing diabetic wound healing. As shown in Fig. 1d, larger amounts of newly formed blood vessels were observed in hucMSC-EV-treated wounds at day 12 post-wounding compared with PBS-treated wounds. The percentage vessel area in hucMSC-EV-treated wounds was significantly higher than that in PBS-treated wounds (Figure S8). The blood flow at wound sites in different groups was evaluated by small animal doppler. Flux images of hucMSC-EV-treated wounds showed larger red areas than control wounds (Fig. 1e), reflecting better blood perfusion in hucMSC-EV-treated wounds. The mean perfusion unit (MPU) ratio in hucMSC-EV-treated mice was also higher than that in control mice (Figure S9). CD31 is a marker for newly formed blood vessels. Immunohistochemistry for CD31 (Fig. 1f) revealed that newly developed blood vessels at wound sites were increased following treatment with hucMSC-EVs compared with controls from day 4 to day 8 (Figure S10). Collectively, these findings suggested that hucMSC-EVs can promote angiogenesis at wound sites in diabetic mice.

HucMSC-EVs Improve the Function of HG-treated HUVECs in Vitro

To understand the multiple effects of hucMSC-EVs on HUVECs, we first determined whether hucMSC-EVs could be internalized into endothelial cells. Previous studies illustrated that adhesion molecules on the surface of EVs are associated with adherence to specific cells, but the cellular and molecular bases for specific targeting of recipient cells remain unclear. Therefore, we tested whether hucMSC-EVs could be taken up by HUVECs. HucMSC-EVs were labeled with PKH67 and then incubated with HUVECs. Next, recipient HUVECs were washed with PBS to remove unbound labeled EVs. After fixation with paraformaldehyde, recipient cells were stained with CD31 (red) and 4′,6-diamidino-2-phenylindole. As shown in Fig. 2a, all HUVECs were stained green after incubation with labeled hucMSC-EVs for 4.5 h, demonstrating that PKH67-tagged hucMSC-EVs had been transferred to the perinuclear regions of HUVECs.

To simulate a HG microenvironment *in vitro*, HUVECs were treated with D-glucose at a final concentration of 35 mM as previously described [37]. The results of a cell counting kit-8 (CCK-8) assay showed lower proliferation of HG-treated HUVECs compared with normal glucose (NG)-treated HUVECs (Fig. 2b). Different concentrations of EVs were added to the culture medium of HG-induced HUVECs. Treatment with hucMSC-EVs significantly enhanced the viability of HG-induced HUVECs at 3, 5 and 7 days in a dose-dependent manner ranging from 6.15×10^8 particles /mL to 2.25×10^9 particles /mL (Figure S11). The 2.25×10^9 particles /mL concentration of hucMSC-EVs had the greatest impact on cell viability (Fig. 2b). This result was further confirmed using a cell cycle assay. The proportions of three cellular subpopulations (G_0/G_1, S and G_2/M) were estimated from DNA distribution as determined by flow cytometry. HG stimulation inhibited the G_1-S transition, and treatment with hucMSC-EVs partially rescued HG-induced cell cycle arrest. In HG + hucMSC-EV-treated HUVECs, more cells were in the S and G_2/M phases compared with HUVECs treated with HG alone, suggesting that hucMSC-EVs promoted entry into the proliferative phase (Fig. 2c, d). Migration of HUVECs was evaluated using wound scratch and transwell assays. Scratch assays demonstrated that the migration rates of HG-induced HUVECs were decreased significantly compared with NG-induced HUVECs. However, hucMSC-EV stimulation improved the migration rates of HG-treated HUVECs (Fig. 2e, f). Consistent with the results of the scratch assay, the number of migrated HG-treated HUVECs was less than the number of migrated NG-treated HUVECs. Following treatment with hucMSC-EVs, the number of migrated cells was increased (Fig. 2g, h). The tube formation assay conducted on Matrigel is a model of angiogenesis *in vitro*. As shown in Fig. 2i, the number of capillary-like structures was decreased in HG-treated HUVECs compared with NG-treated HUVECs. The number of capillary-like structures formed by HG-treated HUVECs increased after incubation with hucMSC-EVs. Quantitative measurements showed that total branch points and total branching length were significantly increased after incubation of HG-treated HUVECs with hucMSC-EVs (Fig. 2j). These results indicated that hucMSC-EVs promoted proliferation, migration, and tube formation in HG-treated HUVECs.

HucMSC-EVs are Enriched with miR-17-5p Targeting PTEN/AKT/HIF-1α/VEGF Pathway

EVs contain a large number of information-containing molecules including miRNAs that can be transferred to target cells to modulate cellular function [35]. We hypothesized that miRNAs in hucMSC-EVs may be conveyed into HUVECs to improve the function of HG-treated HUVECs. To explore the miRNAs within hucMSC-EVs that may be involved in angiogenesis, we examined miRNA expression in EVs using a miRNA microarray. Figure S3 showed the detectable miRNAs in hucMSC-EVs (value > 0). The four most abundant miRNAs were miR-17-5p, miR-3960, miR-4497, and let-7d-5p, which accounted for 10.0 %, 6.0 %, 5.8 %, and 4.1 % of total miRNA reads (Fig. 3a). qRT-PCR was performed to detect a group of miRNAs (miR-17-3p/5p, miR-21-3p/5p, miR-125-3p/5p, miR-19-3p/5p, miR-27-3p/5p, miR-214-3p/5p) which were reported to play roles in

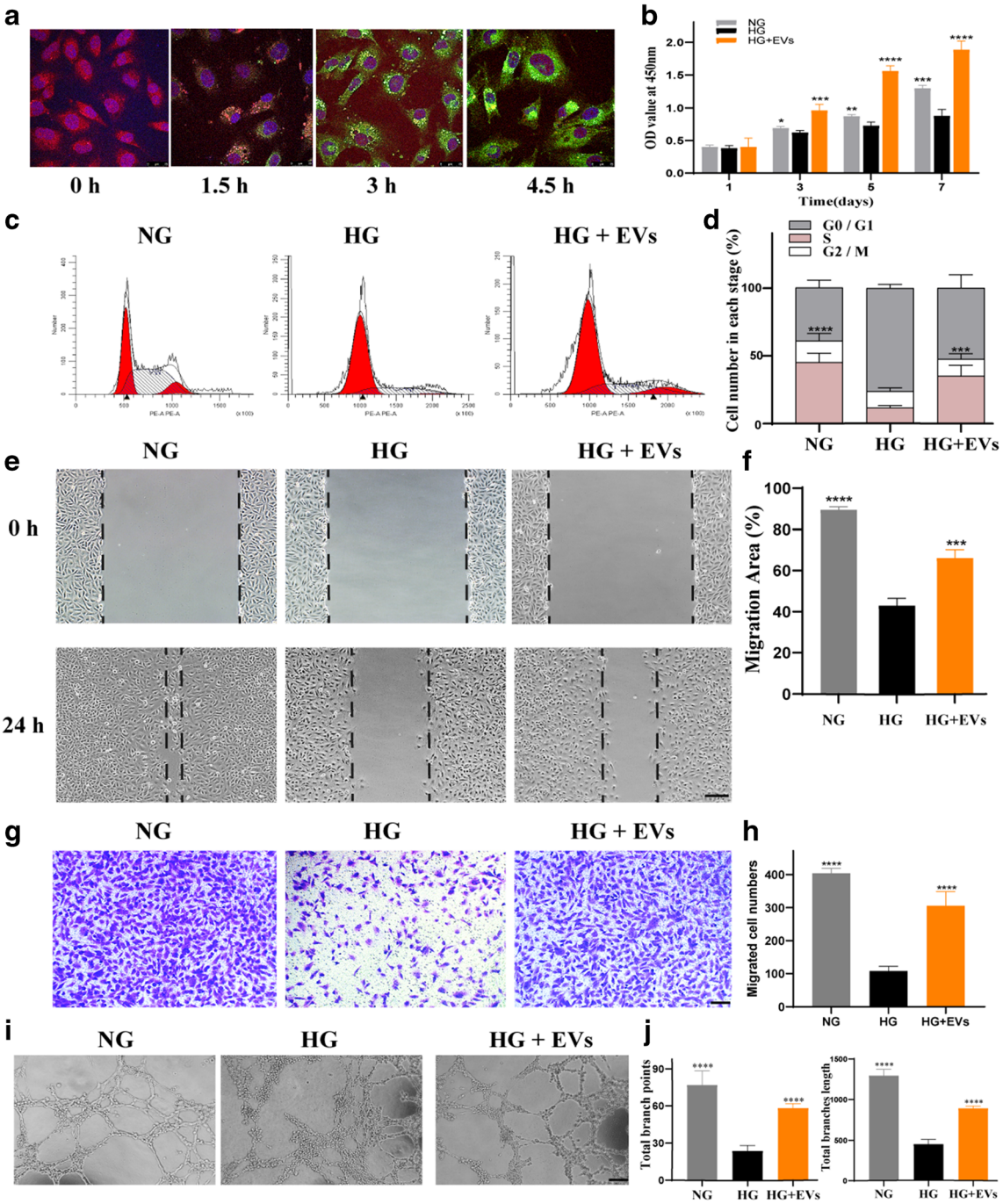

Fig. 2 HucMSC-EVs improve the function of HG-treated HUVECs in vitro. **a** Laser confocal images of HUVECs that were co-cultured with PKH67-labeled hucMSC-EVs (green). CD31 antibody (red) and DPAI (blue)were used to marked the cells. The observation timing is indicated below the images. Scale Bar: 25 μm. **b** CCK-8 analysis was conducted to estimate the proliferation of HUVEC incubated with NG, HG and HG + hucMSC-EVs. *$p < 0.05$, **$p < 0.01$, ***$p < 0.001$, ****$p < 0.0001$. **c-d** Effects of hucMSC-EVs on the cell cycle progression of HG-treated HUVECs (n = 5 for each group). ***$p < 0.001$, ****$p < 0.0001$. **e-h** Cell scratch assay and transwell assay were performed to assess the migration ability of HUVECs from different groups, as well as quantitative analysis. Scale Bar: 100 μm. ***$p < 0.001$, ****$p < 0.0001$. **i** The images of tube formation of HUVECs with different treatments. Scale Bar: 100 μm. **j** Quantitative analysis of tube formation ability, ****$p < 0.0001$

regulating endothelial cell function in vitro and/or angiogenesis in vivo. The results confirmed the presence of the selected miRNAs in hucMSC-EVs. Consistent with the results of miRNA microarrays, miR-17-5p had the highest expression among the detected microRNAs (Fig. 3b). Although studies of miR-17-5p in tumor development abound, studies of the role of this miRNA in wound healing are not reported. Therefore, we focused on miR-17-5p in EVs for further experiments. By

searching Targetscan, miRanda and Pictar, PTEN mRNA (mPTEN) was found to contain a putative miR-17-5p binding site in the 3'-untranslated regions (nucleotides 272–278, Fig. 3c). Besides literature have substantiated PTEN was a target gene silenced by miR-17-5p [38, 39].

PTEN is well known to be an upstream regulator of the AKT/ HIF-1α/VEGF pathways, restricting cell growth and motility signaling by inhibiting phosphorylation of AKT [40]. It was reported that phosphorylation of AKT can increase the expression of HIF-1α and that VEGF is the most important proangiogenic target of HIF-1α [41]. Previous studies showed that the PTEN/AKT/HIF-1α/VEGF pathways played important roles in processes related to angiogenesis [42, 43]. Therefore, we explored whether miR-17-5p could target PTEN to activate AKT/HIF-1α/VEGF signaling pathway. First, we produced EVs lacking miR-17-5p by transfecting hucMSCs with miR-17-5p inhibitors [44] and the average transfection rate was 91.53 % (Figure S12). EVs isolated from hucMSCs transfected with miR-17-5p inhibitors were named EVs-inhibitor$^{miR-17-5p}$ and those isolated from hucMSCs transfected with negative control (NC) inhibitors were named EVs-inhibitor^{NC} and the average transfection rate was 97.92 % (Figure S13). EVs-inhibitor$^{miR-17-5p}$ or EVs-inhibitor^{NC} were used to treat HG-induced HUVECs. Besides, HG-induced HUVECs were transfected with miR-17-5p agomirs or NC agomirs. qRT-PCR analysis showed that miR-17-5p expression was decreased in EVs-inhibitor$^{miR-17-5p}$-treated HUVECs compared with EVs-inhibitor^{NC}-treated HUVECs ($p < 0.05$), whereas a significant increase in miR-17-5p expression in miR-17-5p agomir-

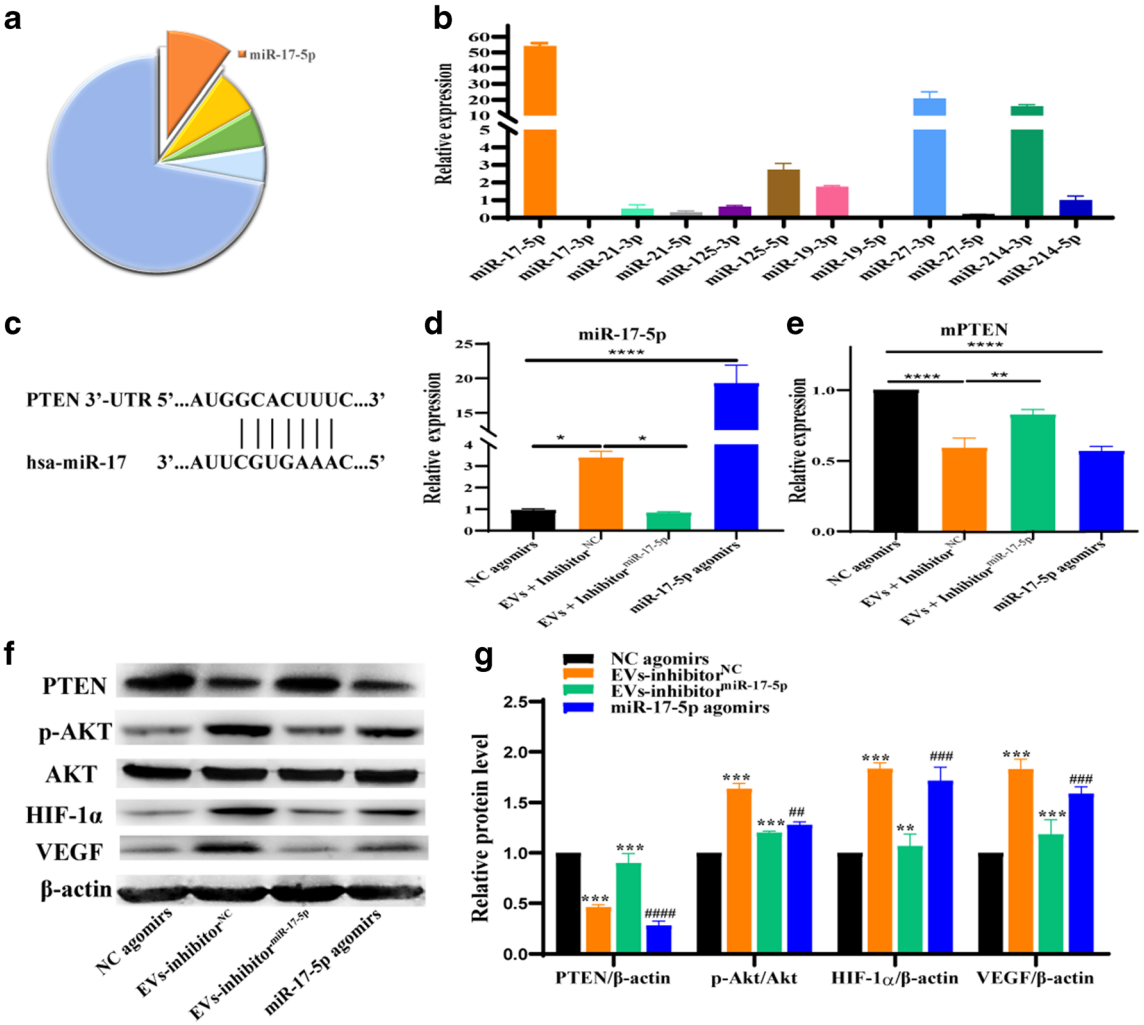

Fig. 3 MiR-17-5p in hucMSC-EVs downregulates PTEN and activates AKT/HIF-1α/VEGF pathway in HG-treated HUVECs. **a** Proportion of miRNAs in total miRNA reads. **b** Detection of the expression of the indicated miRNAs by qRT-PCR analysis (n = 3 per group). **c** Putative miR-17-5p binding sites(red) in the 3' - UTRs of PTEN. **d** The miR-17-5p expression levels in HUVECs treated with NC agomirs, EVs-inhibitor^{NC}, EVs-inhibitor $^{miR-17-5p}$, and miR-17-5p agomirs. *$p < 0.05$, ***$p < 0.001$. **e** Expression of mPTEN in HUVECs after incubation with NC agomirs, EVs-inhibitor^{NC}, EVs-inhibitor $^{miR-17-5p}$, and miR-17-5p agomirs for 24 h (n = 3 per group). *$p < 0.05$, ****$p < 0.0001$. **f-g** The expression level of PTEN, p-AKT, HIF-1α, and VEGF and the quantification results. The results of PTEN, HIF-1α, and VEGF are normalized to β-actin expression and the result of p-AKT is normalized to AKT expression (n = 3 per group). ***$p < 0.001$, ****$p < 0.0001$

transfected cells, but not in NC agomir-transfected cells ($p < 0.001$) (Fig. 3d), was found. As expected, hucMSC-EVs lacking miR-17-5p did not suppress PTEN mRNA expression. By contrast, miR-17-5p agomirs significantly suppressed PTEN mRNA levels ($p < 0.0001$), similar to the effects of hucMSC-EVs (Fig. 3e). Furthermore, protein expression of PTEN, p-AKT, AKT, HIF-1α, and VEGF was also assessed by western blotting and showed results consistent with mRNA levels (Fig. 3f, g). Thus, hucMSC-EVs treatment promoted the expression of p-AKT, HIF-1α and VEGF ($p < 0.0001$), whereas their up-regulation was reduced in EVs-inhibitor$^{miR-17-5p}$-treated HUVECs ($p < 0.001$). EV-like up-regulation could be induced by a miR-17-5p agomir. Collectively, these data demonstrated that miR-17-5p in hucMSC-EVs could activate AKT/HIF-1α/VEGF signaling by down-regulating PTEN expression.

MiR-17-5p in HucMSC-EVs Promotes Proliferation, Migration and Tube Formation of HG-Treated HUVECs

Subsequently, we investigated the proliferation, migration, and tube formation of HG-treated HUVECs treated or transfected with NC agomirs, EVs-inhibitor^{NC}, EVs-inhibitor$^{miR-17-5p}$, and miR-17-5p agomirs. CCK-8 assays revealed that EVs-inhibitor^{NC} treatment and miR-17-5p agomir transfection significantly enhanced the proliferative capacity of HG-induced HUVECs (Fig. 4a). The miR-17-5p agomir partially mimicked the effects of EVs-inhibitor^{NC} on the proliferation of HG-induced HUVECs, indicating that other molecules within hucMSC-EVs may be involved in regulating the cellular function of HG-induced HUVECs (Fig. 4a). Next, the wound scratch and transwell assays were used to evaluate the properties of HG-induced HUVECs treated or transfected with EVs or miRNA agomirs. The cellular migration area was significantly increased in EVs-inhibitor^{NC}-treated HUVECs ($p < 0.0001$), whereas EVs-inhibitor$^{miR-17-5p}$ treatment showed no such effect. MiR-17-5p agomirs partially mimicked the effect EVs-inhibitor^{NC} in enhancing cellular migration ($p < 0.0001$) compared with NC agomirs (Fig. 4b, c). A transwell assay further confirmed these effects on cell migration. The numbers of migrated EVs-inhibitor^{NC}-treated HUVECs ($p < 0.0001$) and miR-17-5p agomir-transfected HUVECs ($p < 0.0001$) were enhanced compared with those of EVs-inhibitor$^{miR-17-5p}$-treated HUVECs and NC agomir-transfected HUVECs (Fig. 4d, e). The total branching points and total tube length were calculated to evaluate the angiogenic ability of HG-induced HUVECs treated or transfected with EVs or miRNA agomirs. The total numbers of branching points ($p < 0.001$) and total tube length ($p < 0.0001$) were increased in miR-17-5p agomir-transfected HUVECs compared with NC agomir-transfected HUVECs (Fig. 4f, g). Moreover, tube formation in EVs-inhibitor$^{miR-17-5p}$-treated HUVECs was markedly reduced compared with EVs-inhibitor^{NC}-treated HUVECs. Thus, hucMSC-EVs could improve the function of endothelial cells by targeting the PTEN/AKT/HIF-1α/VEGF signaling pathways through miR-17-5p.

MiR-17-5p in HucMSC-EVs Exerts Angiogenic Effects on Wound Healing in Diabetic Mice

Finally, we sought to evaluate the ability of miR-17-5p to facilitate wound healing of diabetic mice *in vivo*. Full-thickness wounds on the back were locally injected with NC agomirs, EVs-inhibitor^{NC}, EVs-inhibitor$^{miR-17-5p}$, or miR-17-5p agomirs every other day post wounding. As showed in Fig. 5a, the wound healing process was significantly accelerated by local injection of EVs-inhibitor^{NC} compared with EVs-inhibitor$^{miR-17-5p}$, and was also enhanced by miR-17-5p agomirs compared with NC agomirs (Figure S14). Higher local MPU ratios were also observed in EVs-inhibitor^{NC} and miR-17-5p agomir-treated mice, reflecting enhanced blood flow at wound sites ($p < 0.05$) (Fig. 5b, S15). Consistent with the wound healing and MPU ratio analyses, EVs-inhibitor^{NC} and miR-17-5p agomirs significantly increased the numbers of newly formed blood vessels ($p < 0.0001$) (Fig. 5c, S16) and CD31 expression levels ($p < 0.001$) (Fig. 5d, e). Furthermore, EVs-inhibitor^{NC} induced improvements in angiogenesis that were diminished by treatment with EVs-inhibitor$^{miR-17-5p}$ (Fig. 5c-e, S15-16). Collectively, these findings revealed that miR-17-5p plays a crucial role in hucMSC-EVs-dependent regulation of endothelial angiogenesis: suppression of miR-17-5p in hucMSC-EVs markedly decreased the regulatory effects of hucMSC-EVs, suggesting that these EVs could represent novel therapeutic tools to promote diabetic wound healing.

Discussion

In the present study, we investigated the properties of hucMSC-EVs and their ability to enhance diabetic wound healing and angiogenesis. Potential underlying mechanisms were also explored including signaling in recipient cells and candidate miRNAs in hucMSC-EVs. Our results showed that hucMSC-EVs promoted diabetic wound healing and angiogenesis *in vivo*. *In vitro*, hucMSC-EVs facilitated proliferation, migration, and tube formation in HG-treated HUVECs, and mitigated the cellular senescence induced by HG. The AKT/HIF-1α/VEGF signaling pathways regulated by PTEN were activated by hucMSC-EVs in HG-treated HUVECs. Moreover, inhibition of PTEN mimicked the effects of hucMSC-EVs on endothelial cell function. MiR-17-5p was highly enriched in hucMSC-EVs. Using inhibitors and agomirs, we confirmed that miR-17-5p was a key player in the regulatory effects of hucMSC-EVs on diabetic wound

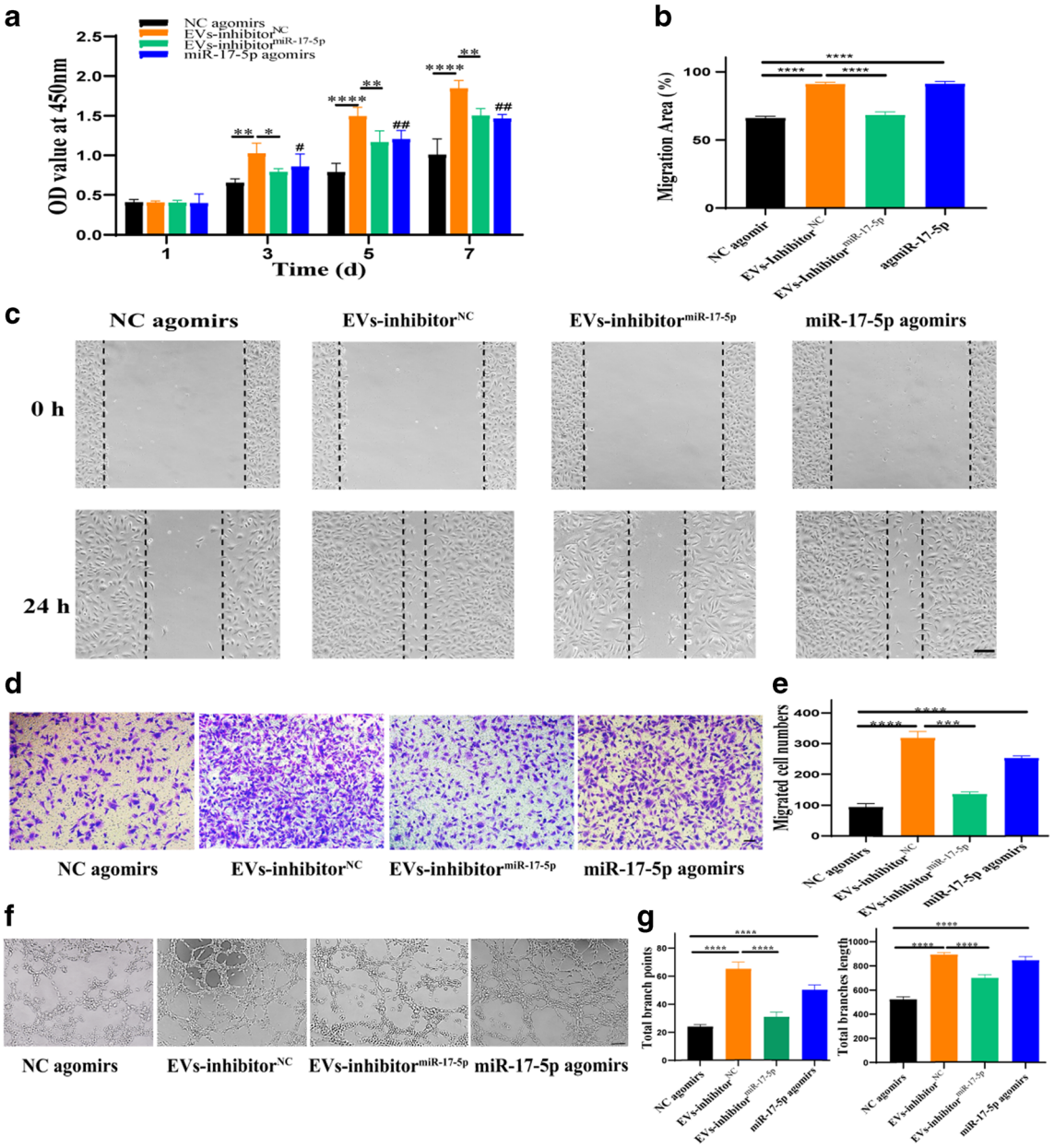

Fig. 4 MiR-17-5p in hucMSC-EVs promotes proliferation, migration and tube formation of HG-treated HUVECs.**a** Proliferation rates of HUVECs from NC agomirs, EVs-inhibitor^{NC}, EVs-inhibitor $^{miR-17-5p}$, and miR-17-5p agomirs groups were measured by CCK-8 assay. *p < 0.05, **p < 0.01, ****p < 0.0001; $^{\#}$p < 0.05, $^{\#\#}$p < 0.01 miR-17-5p agomirs vs. NC agomirs. **b-c** Migration ability of HG-induced HUVECs with different treatments was measured by wound scratch assay (n = 5 per group). Scale Bar: 100 μm, ****p < 0.0001. **d-e** Migration ability of HG-induced HUVECs measured by transwell migration assay (n = 5 per group). Scale Bar: 100 μm. ***p < 0.001, ****p < 0.0001. **f** Effects of different treatments on the tube formation ability of HG-induced HUVECs. Scale Bar: 100 μm. **g** Total branch points and tube length were quantified using ImageJ software (n = 5 per group). ****p < 0.0001

healing and angiogenesis, and exerted its effects by targeting PTEN.

Diabetic wounds are difficult to heal because of their complex underlying pathology. Many studies have showed that angiogenesis is important for wound healing. But in diabetes, persistent hyperglycemia impairs angiogenesis by damaging endothelial function, eventually leading to diabetic ischemia ulcer in clinic such as diabetic foot ulcers and diabetic leg ulcers [8, 9]. The characters of these ulcers include taking a long time to heal, exhibiting prolonged inflammation, and leading to high disability. In China, the incidence of diabetic ischemia ulcers is much higher than that of developed countries in the West [45]. Therefore significant attention has been paid to the treatment of diabetic wound [46]. Stem cells have been reported to have beneficial effects on diabetic wound repair [47]. However, because stem cell transplantation is

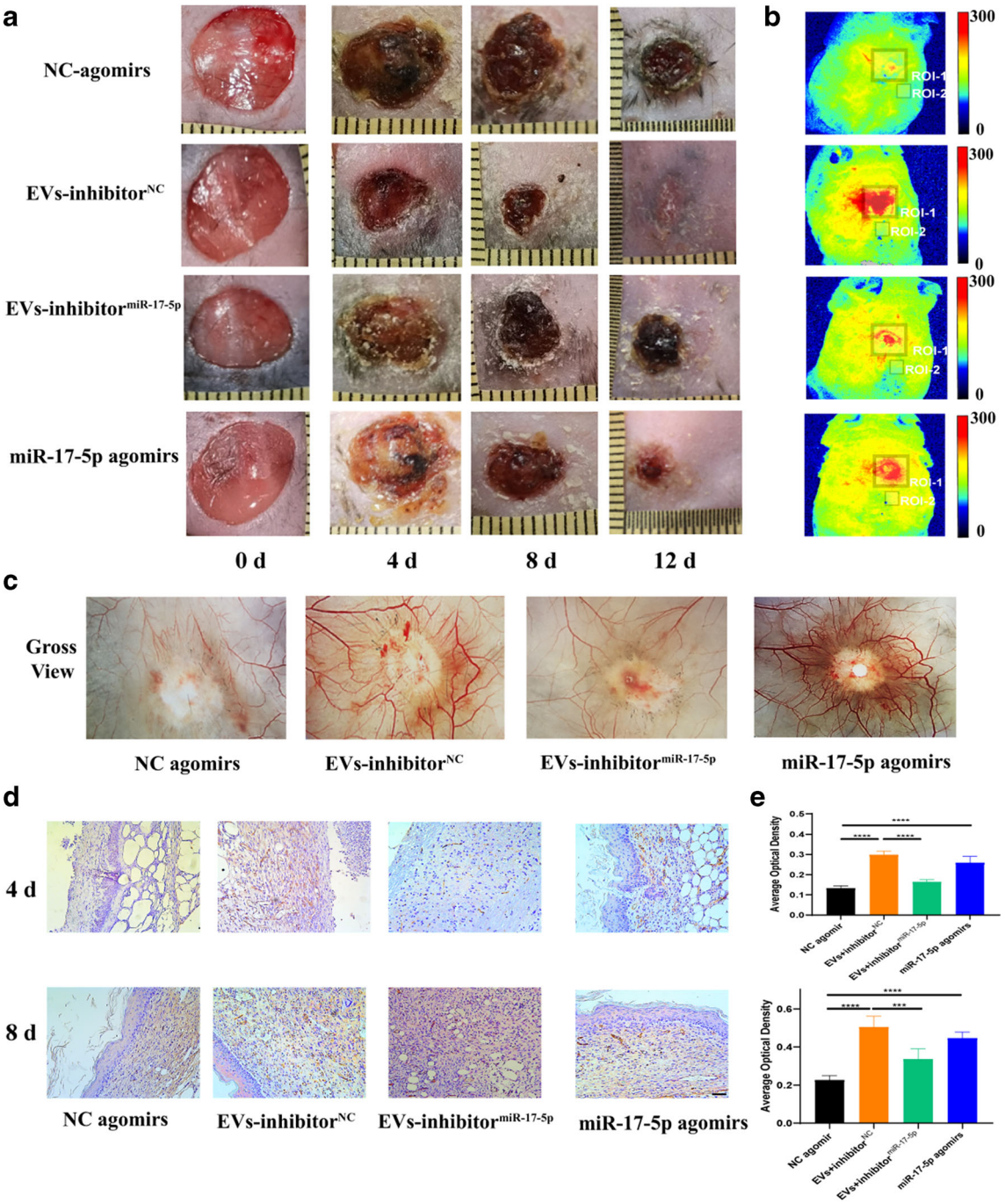

Fig. 5 MiR-17-5p in hucMSC-EVs exerts angiogenic effects on wound healing in diabetic mice.**a** Gross view of wounds from NC agomirs, EVs-inhibitor^{NC}, EVs-inhibitor $^{miR-17-5p}$, and miR-17-5p agomirs groups at day 0, 4, 8 and 12 post wounding. **b** The blood flows at the wound sections of different groups were evaluated by doppler of animals. Flux images of wounds were imaged. **c** Gross view of wounds that received different treatments at day 12 post wounding. Vascularization was found in the wound sections. **d** CD31 staining of wound sites in every group at day 4 and day 8 post wounding. Scale bar: 100 μm. **e** Quantitation of average optical density (AOD) of wound sites in different groups (n = 5 per group). ***p < 0.001, ****p < 0.0001

limited by immune rejection, tumorigenicity, and ethical issues, this therapy is not widely available in the clinic. Recent studies have found that culture supernatants of stem cells can accelerate the repair of damaged tissue [48, 49]. Accordingly, researchers are beginning to focus upon the exocrine function of stem cells. EVs are key paracrine factors of stem cells that can modulate the functions of target cells in wound healing. For treatment of diabetic wounds, MSC-derived EVs are receiving more and more attention. Recently, we reported that EVs from human decidua-derived MSCs could enhance

diabetic wound healing by optimizing functional states of fibroblasts [50]. In the current study, we showed the beneficial effects of hucMSC-EVs on diabetic wound healing.

During wound healing, the formation of new blood vessels is crucial for delivering trophic factors to wound sites [51]. Under the hyperglycemic conditions of diabetes, glucose toxicity can lead to reduced cellular viability and increased senescence of endothelial cells [52], resulting in insufficient angiogenesis and low capillary density in diabetic wounds. Therefore, endothelial cells may be potential targets for ameliorating diabetic vascular complications. Using a rat skin burn model, Zhang et al. demonstrated that hucMSC-EVs promoted wound healing and angiogenesis *in vivo* via the Wnt4/β-catenin pathway [53]. Under HG conditions, the functional states of endothelial cells differ from those under NG conditions, so whether hucMSC-EVs can perform a similar function needs to be confirmed. In the present study, we demonstrated that treatment with hucMSC-EVs boosted neovascularization in diabetic wounds. Using a suite of *in vitro* angiogenesis-related assays, we discovered that hucMSC-EVs could profoundly stimulate proliferation, migration and angiogenic tube formation of HG-treated HUVECs. These experiments confirmed the pro-angiogenic properties of hucMSC-EVs. Thus, the favorable effects of hucMSC-EVs on diabetic wound healing may be ascribed to their function in restoration of injured endothelial cells under HG conditions.

We next investigated the mechanism responsible for the regenerative function of hucMSC-EVs on HG-treated HUVECs. MiRNAs are short RNA molecules that play vital roles in a wide array of biological processes [54]. MiRNAs are secreted into the extracellular space within EVs, allowing for their transfer to recipient cells where they can mediate gene expression [55]. In this study, the candidate miRNAs within hucMSC-EVs were identified using miRNA microarrays and qRT-PCR. We found that miR-17-5p was highly enriched in hucMSC-EVs. MiR-17-5p has been proved to regulate angiogenesis [56]. For example, miR-17 from endothelial cells enhanced angiogenesis in renal ischemia-reperfusion injury [57]. By contrast, in colorectal cancer, miR-17 ~ 92 suppressed angiogenesis thereby inhibiting cancer progression. Thus, the pro- or anti- angiogenic effects of miR-17-5p may be cellular or tissue context-dependent. However, in diabetic wounds, the functions of miR-17-5p derived from hucMSC-EVs in angiogenesis remain unclear. We incubated HUVECs with hucMSC-EVs and found that the expression of miR-17-5p was remarkably enhanced. Administration of a specific inhibitor targeting miR-17-5p reversed, but did not entirely abolish, the effects of hucMSC-EVs on angiogenesis in vitro and in vivo. Moreover, agomirs of miR-17-5p could partially simulate the effects of hucMSC-EVs. On the basis of our findings, we propose that miR-17-5p is one of the principal mediators of hucMSC-EV-induced regulation of endothelial cell properties. However, other signaling regulator may also be associated with this process, and will require further investigation.

Our study also confirmed the connection between the activated signaling pathways in recipient cells and mediators within EVs. The AKT/HIF-1α/VEGF pathways have been demonstrated to augment several crucial processes associated with angiogenesis such as migration and tube formation of endothelial cells [58]. PTEN is reported as a negative regulator of the AKT/HIF-1α/VEGF pathways [59]. Previous studies have demonstrated that the effects of miR-17-5p were mediated via inhibiting PTEN and increasing Akt kinase activity [39, 60]. In agreement with these findings, our results showed that the inhibitors of miR-17-5p attenuated enhanced expression of PTEN and p-Akt induced by hucMSC-EVs. In contrast, agomirs of miR-17-5p functioned as well as hucMSC-EVs to increase the expression of PTEN and p-Akt. Bioinformatic analyses supported the finding that PTEN is a direct target of miR-17-5p. We conclude that high levels of miR-17-5p in hucMSC-EVs are responsible for modulating angiogenesis in diabetic wounds by targeting PTEN and activating the AKT/HIF-1α/VEGF pathways in HG-injured endothelial cells.

Conclusions

In conclusion, our findings demonstrate that hucMSC-EVs can potently better cutaneous wound repair in diabetic mice and the determining mechanism could be their enhancement of pro-angiogenic properties of endothelial cells in the diabetic wound sites, as hucMSC-EVs can boost the proliferation, migration and the angiogenic activities of HG-pretreated HUVECs. These therapeutic effects are proved to be miR-17-5p-dependent, for the inhibition of miR-17-5p can significantly attenuate the hucMSC-EVs-induced impacts and agmirR-17-5p can partly achieve hucMSC-EVs-like effects. Moreover, miR-17-5p exerts functions directly via manipulating PTEN/AKT/HIF-1α/VEGF signaling pathway. It will also be of interest to analyze whether hucMSC-EVs have positive effects on the function of other cell types in diabetic wounds. These results confirmed the value of hucMSC-EVs to meditate therapeutic miRNAs and suggested the efficacy of this strategy in diabetic wound management merited further investigation.

Supplementary Information The online version contains supplementary material available at https://doi.org/10.1007/s12015-021-10176-0.

Author Contributions QW: design and performance of the in vivo and in vitro studies, result analysis and writing original manuscript draft; YW: in vivo transplantation and imaging studies; KM: preparation of the cells and in vitro studies; XB: EV studies and imaging; QL: RNA interference;

BL: blood perfusion evaluation; WH: cell function evaluation; XF and CZ: design, result analysis, manuscript writing and editing, and funding acquisition. All authors have read and approved the final manuscript draft.

Funding This work was supported by the National Nature Science Foundation of China (81830064, 81721092, 81901971); the National Key Research Development Plan (2017YFC1103304); the CAMS Innovation Fund for Medical Sciences (CIFMS, 2019-I2M-5-059); the Military Medical Research and Development Projects (AWS17J005, 2019 − 126) and the Beijing Municipal Natural Science Foundation (7202197, 7194316).

Data Availability The datasets used and/or analyzed during the current study are available from the corresponding author on reasonable request.

Code Availability Not applicable.

Declarations

Ethics Approval and Consent to Participate All animal procedures were approved by the Animal Research Committee of PLA General Hospital and were performed in accordance with established guidelines.

Consent for Publication Not applicable.

Conflict of Interest The authors have declared that no competing interest exists.

Supplementary Information The online version contains supplementary material available at https://doi.org/10.1007/s12015-021-10176-0.

References

1. Patel, S., Srivastava, S., Singh, M. R., & Singh, D. (2019). Mechanistic insight into diabetic wounds: Pathogenesis, molecular targets and treatment strategies to pace wound healing. *Biomedicine and Pharmacotherapy, 112*, 108615.
2. Fu, X., Sheng, Z., Cherry, G. W., & Li, Q. (1998). Epidemiological study of chronic dermal ulcers in China. *Wound Repair and Regeneration, 6*, 21–27.
3. Jiang, Y., Huang, S., Fu, X., Liu, H., Ran, X., Lu, S., et al. (2011). Epidemiology of chronic cutaneous wounds in China. *Wound Repair and Regeneration, 19*, 181–188.
4. Jeffcoate, W. J., & Harding, K. G. (2003). Diabetic foot ulcers. *Lancet, 361*, 1545–1551.
5. Kant, V., Gopal, A., Kumar, D., Pathak, N. N., Ram, M., Jangir, B. L., Tandan, S. K., & Kumar, D. (2015). Curcumin-induced angiogenesis hastens wound healing in diabetic rats. *Journal of Surgical Research, 193*, 978–988.
6. Bakker, K., Apelqvist, J., Lipsky, B. A., & Van Netten, J. J. (2016). The 2015 IWGDF guidance documents on prevention and management of foot problems in diabetes: development of an evidence-based global consensus. *Diabetes/Metabolism Research and Reviews, 32*(Suppl 1), 2–6.
7. Galkowska, H., Wojewodzka, U., & Olszewski, W. L. (2006). Chemokines, cytokines, and growth factors in keratinocytes and dermal endothelial cells in the margin of chronic diabetic foot ulcers. *Wound Repair and Regeneration, 14*, 558–565.
8. Falanga, V. (2005). Wound healing and its impairment in the diabetic foot. *Lancet, 366*, 1736–1743.
9. Wu, Y. S., & Chen, S. N. (2016). Extracted triterpenes from antrodia cinnamomea reduce the inflammation to promote the wound healing via the STZ inducing hyperglycemia-diabetes mice model. *Frontiers in Pharmacology, 7,* 154.
10. Samsonraj, R. M., Raghunath, M., Nurcombe, V., Hui, J. H., van Wijnen, A. J., & Cool, S. M. (2017). Concise review: multifaceted characterization of human mesenchymal stem cells for use in regenerative medicine. *Stem Cells Transl Med, 6,* 2173–2185.
11. Kim, S. M., Kim, Y. H., Jun, Y. J., Yoo, G., & Rhie, J. W. (2016). The effect of diabetes on the wound healing potential of adipose-tissue derived stem cells. *International Wound Journal, 13*(Suppl 1), 33–41.
12. Kim, E. K., Li, G., Lee, T. J., & Hong, J. P. (2011). The effect of human adipose-derived stem cells on healing of ischemic wounds in a diabetic nude mouse model. *Plastic and Reconstructive Surgery, 128*, 387–394.
13. Chen, Y., Zhao, Y., Chen, W., Xie, L., Zhao, Z. A., Yang, J., Chen, Y., Lei, W., & Shen, Z. (2017). MicroRNA-133 overexpression promotes the therapeutic efficacy of mesenchymal stem cells on acute myocardial infarction. *Stem Cell Research & Therapy, 8*, 268.
14. Zhao, J., Li, X., Hu, J., Chen, F., Qiao, S., Sun, X., Gao, L., Xie, J., & Xu, B. (2019). Mesenchymal stromal cell-derived exosomes attenuate myocardial ischaemia-reperfusion injury through miR-182-regulated macrophage polarization. *Cardiovascular Research, 115*, 1205–1216.
15. Shiota, Y., Nagai, A., Sheikh, A. M., Mitaki, S., Mishima, S., Yano, S., Haque, M. A., Kobayashi, S., & Yamaguchi, S. (2018). Transplantation of a bone marrow mesenchymal stem cell line increases neuronal progenitor cell migration in a cerebral ischemia animal model. *Scientific Reports, 8*, 14951.
16. Hawkins, K. E., Corcelli, M., Dowding, K., Ranzoni, A. M., Vlahova, F., Hau, K. L., et al. (2018). Embryonic stem cell-derived Mesenchymal Stem Cells (MSCs) have a superior neuroprotective capacity over fetal MSCs in the hypoxic-ischemic mouse brain. *Stem Cells Translational Medicine, 7,* 439–449.
17. Wang, Z., Zheng, L., Lian, C., Qi, Y., Li, W., & Wang, S. (2019). Human umbilical cord-derived mesenchymal stem cells relieve hind limb ischemia by promoting angiogenesis in mice. *Stem Cells and Development, 28,* 1384–1397.
18. Shen, L., Zeng, W., Wu, Y. X., Hou, C. L., Chen, W., Yang, M. C., Li, L., Zhang, Y. F., & Zhu, C. H. (2013). Neurotrophin-3 accelerates wound healing in diabetic mice by promoting a paracrine response in mesenchymal stem cells. *Cell Transplantation, 22*, 1011–1021.
19. Wang, S., Yang, H., Tang, Z., Long, G., & Huang, W. (2016). Wound dressing model of human umbilical cord mesenchymal stem cells-alginates complex promotes skin wound healing by paracrine signaling. *Stem Cells International, 2016*, 3269267.
20. Jung, J. W., Kwon, M., Choi, J. C., Shin, J. W., Park, I. W., Choi, B. W., & Kim, J. Y. (2013). Familial occurrence of pulmonary embolism after intravenous, adipose tissue-derived stem cell therapy. *Yonsei Medical Journal, 54*, 1293–1296.
21. Barkholt, L., Flory, E., Jekerle, V., Lucas-Samuel, S., Ahnert, P., Bisset, L., et al. (2013). Risk of tumorigenicity in mesenchymal stromal cell-based therapies–bridging scientific observations and regulatory viewpoints. *Cytotherapy, 15*, 753–759.
22. Furlani, D., Ugurlucan, M., Ong, L., Bieback, K., Pittermann, E., Westien, I., et al. (2009). Is the intravascular administration of mesenchymal stem cells safe? Mesenchymal stem cells and intravital microscopy. *Microvascular Research, 77*, 370–376.
23. Lamichhane, T. N., Sokic, S., Schardt, J. S., Raiker, R. S., Lin, J. W., & Jay, S. M. (2015). Emerging roles for extracellular vesicles in tissue engineering and regenerative medicine. *Tissue Engineering. Part B, Reviews, 21,* 45–54.
24. Ti, D., Hao, H., Tong, C., Liu, J., Dong, L., Zheng, J., et al. (2015). LPS-preconditioned mesenchymal stromal cells modify

macrophage polarization for resolution of chronic inflammation via exosome-shuttled let-7b. *Journal of Translational Medicine, 13*, 308.
25. Liang, X., Zhang, L., Wang, S., Han, Q., & Zhao, R. C. (2016). Exosomes secreted by mesenchymal stem cells promote endothelial cell angiogenesis by transferring miR-125a. *Journal of Cell Science, 129*, 2182–2189.
26. Xiong, Y., Chen, L., Yan, C., Zhou, W., Endo, Y., Liu, J., et al. (2020). Circulating exosomal miR-20b-5p inhibition restores Wnt9b signaling and reverses diabetes-associated impaired wound healing. *Small (Weinheim an der Bergstrasse, Germany), 16,* e1904044.
27. Yang, J., Chen, Z., Pan, D., Li, H., & Shen, J. (2020). Umbilical cord-derived mesenchymal stem cell-derived exosomes combined pluronic F127 hydrogel promote chronic diabetic wound healing and complete skin regeneration. *International Journal of Nanomedicine, 15,* 5911–5926.
28. Jia, G., Han, Y., An, Y., Ding, Y., He, C., Wang, X., & Tang, Q. (2018). NRP-1 targeted and cargo-loaded exosomes facilitate simultaneous imaging and therapy of glioma in vitro and in vivo. *Biomaterials, 178*, 302–316.
29. Coleman, D. L., & Hummel, K. P. (1967). Studies with the mutation, diabetes, in the mouse. *Diabetologia, 3*, 238–248.
30. Hu, Y., Rao, S. S., Wang, Z. X., Cao, J., Tan, Y. J., Luo, J., et al. (2018). Exosomes from human umbilical cord blood accelerate cutaneous wound healing through miR-21-3p-mediated promotion of angiogenesis and fibroblast function. *Theranostics, 8*, 169–184.
31. Baptista, V. I. A., Quintana, H. T., Lazzarin, M. C., Benfato, I. D., De Carvalho, F. P., Le Sueur-Maluf, L., De Oliveira, C. A. M., Baptista, J. D. S., & De Oliveira, F. (2019). Short time insulin treatment post burn improves elastic-collagen rearrangement and reepithelization. *Connective Tissue Research, 60*, 230–239.
32. Liu, S., Wu, F., Gu, S., Wu, T., Chen, S., Chen, S., et al. (2019). Gene silencing via PDA/ERK2-siRNA-Mediated electrospun fibers for peritendinous antiadhesion. *Advanced Science (Weinheim, Germany), 6,* 1801217.
33. Liu, Z. L., Zhang, J. G., Liu, Q., Yi, L. T., Li, Y. M., & Li, Y. (2017). The vascular protective effects of Anoectochilus roxburghii polysaccharose under high glucose conditions. *Journal of Ethnopharmacology, 202*, 192–199.
34. Kupcova Skalnikova, H. (2013). Proteomic techniques for characterisation of mesenchymal stem cell secretome. *Biochimie, 95*, 2196–2211.
35. Wang, A., Liu, J., Zhuang, X., Yu, S., Zhu, S., Liu, Y., & Chen, X. (2020). Identification and comparison of piRNA expression profiles of exosomes derived from human stem cells from the apical papilla and bone marrow mesenchymal stem cells. *Stem Cells and Development, 29,* 511–520.
36. Bian, X., Li, B., Yang, J., Ma, K., Sun, M., Zhang, C., & Fu, X. (2020). Regenerative and protective effects of dMSC-sEVs on high-glucose-induced senescent fibroblasts by suppressing RAGE pathway and activating Smad pathway. *Stem Cell Research & Therapy, 11*, 166.
37. Maisto, R., Oltra, M., Vidal-Gil, L., Martínez-Gil, N., Sancho-Pellúz, J., Filippo, C., et al. (2019). ARPE-19-derived VEGF-containing exosomes promote neovascularization in HUVEC: the role of the melanocortin receptor 5. *Cell Cycle (Georgetown, Texas), 18,* 413–424.
38. Shi, Y. P., Liu, G. L., Li, S., & Liu, X. L. (2020). miR-17-5p knockdown inhibits proliferation, autophagy and promotes apoptosis in thyroid cancer via targeting PTEN. *Neoplasma, 67*, 249–258.
39. Tian, Y., Li, X., Bai, C., Yang, Z., Zhang, L., & Luo, J. (2020). MiR-17-5p promotes the endothelialization of endothelial progenitor cells to facilitate the vascular repair of aneurysm by regulating PTEN-mediated PI3K/AKT/VEGFA pathway. *Cell Cycle (Georgetown, Texas), 19,* 3608–3621.
40. Worby, C. A., & Dixon, J. E. (2014). PTEN. *Annual Review of Biochemistry, 83*, 641–669.
41. Xiang, T., Lin, Y. X., Ma, W., Zhang, H. J., Chen, K. M., He, G. P., et al. (2018). Vasculogenic mimicry formation in EBV-associated epithelial malignancies. *Nature Communications, 9,* 5009.
42. Park, J. H., Lee, J. Y., Shin, D. H., Jang, K. S., Kim, H. J., & Kong, G. (2011). Loss of Mel-18 induces tumor angiogenesis through enhancing the activity and expression of HIF-1α mediated by the PTEN/PI3K/Akt pathway. *Oncogene, 30*, 4578–4589.
43. He, Z., Chen, A., Rojanasakul, Y., Rankin, G., & Chen, Y. (2016). Gallic acid, a phenolic compound, exerts anti-angiogenic effects via the PTEN/AKT/HIF-1α/VEGF signaling pathway in ovarian cancer cells. *Oncology Reports, 35*, 291–297.
44. Du, W., Zhang, K., Zhang, S., Wang, R., Nie, Y., Tao, H., et al. (2017). Enhanced proangiogenic potential of mesenchymal stem cell-derived exosomes stimulated by a nitric oxide releasing polymer. *Biomaterials, 133*, 70–81.
45. Jiang, Y., Wang, X., Xia, L., Fu, X., Xu, Z., Ran, X., et al. (2015). A cohort study of diabetic patients and diabetic foot ulceration patients in China. *Wound Repair and Regeneration, 23*, 222–230.
46. Berlanga-Acosta, J., Armstrong, D., Schultz, G., & Herrera-Martinez, L. (2014). Chronic wounds with emphasis in diabetic foot ulcers. *BioMed Research International, 2014*, 890352.
47. Maranda, E. L., Rodriguez-Menocal, L., & Badiavas, E. V. (2017). Role of mesenchymal stem cells in dermal repair in burns and diabetic wounds. *Current Stem Cell Research & Therapy, 12,* 61–70.
48. Fouraschen, S. M., Pan, Q., de Ruiter, P. E., Farid, W. R., Kazemier, G., Kwekkeboom, J., et al. (2012). Secreted factors of human liver-derived mesenchymal stem cells promote liver regeneration early after partial hepatectomy. *Stem Cells and Development, 21*, 2410–2419.
49. Ionescu, L., Byrne, R. N., van Haaften, T., Vadivel, A., Alphonse, R. S., Rey-Parra, G. J., et al. (2012). Stem cell conditioned medium improves acute lung injury in mice: in vivo evidence for stem cell paracrine action. *American Journal of Physiology: Lung Cellular and Molecular Physiology, 303*, L967–L977.
50. An, Y., Liu, W. J., Xue, P., Ma, Y., Zhang, L. Q., Zhu, B., et al. (2018). Autophagy promotes MSC-mediated vascularization in cutaneous wound healing via regulation of VEGF secretion. *Cell Death & Disease, 9*, 58.
51. Casado-Díaz, A., Quesada-Gómez, J. M., & Dorado, G. (2020). Extracellular vesicles derived from Mesenchymal Stem Cells (MSC) in regenerative medicine: applications in skin wound healing. *Frontiers in Bioengineering and Biotechnology, 8,* 146.
52. Rezabakhsh, A., Nabat, E., Yousefi, M., Montazersaheb, S., Cheraghi, O., Mehdizadeh, A., et al. (2017). Endothelial cells' biophysical, biochemical, and chromosomal aberrancies in high-glucose condition within the diabetic range. *Cell Biochemistry and Function, 35*, 83–97.
53. Zhang, B., Wu, X., Zhang, X., Sun, Y., Yan, Y., Shi, H., et al. (2015). Human umbilical cord mesenchymal stem cell exosomes enhance angiogenesis through the Wnt4/β-catenin pathway. *Stem Cells Translational Medicine, 4,* 513–522.
54. Rupaimoole, R., & Slack, F. J. (2017). MicroRNA therapeutics: towards a new era for the management of cancer and other diseases. *Nature Reviews: Drug Discovery, 16*, 203–222.
55. Chen, Y., & Pfeifer, A. (2017). Brown fat-derived exosomes: small vesicles with big impact. *Cell Metabolism, 25,* 759–760.
56. Duan, B., Shi, S., Yue, H., You, B., Shan, Y., Zhu, Z., Bao, L., & You, Y. (2019). Exosomal miR-17-5p promotes angiogenesis in nasopharyngeal carcinoma via targeting BAMBI. *Journal of Cancer, 10*, 6681–6692.
57. Chiba, T., Cerqueira, D., Li, Y., Bodnar, A., Mukherjee, E., Pfister, K., et al. (2021). Endothelial-Derived miR-17~92 Promotes Angiogenesis to Protect against Renal Ischemia-Reperfusion

Injury. *Journal of the American Society of Nephrology: JASN, 32*(3), 553–562.

58. Kakinuma, Y., Furihata, M., Akiyama, T., Arikawa, M., Handa, T., Katare, R., & Sato, T. (2010). Donepezil, an acetylcholinesterase inhibitor against Alzheimer's dementia, promotes angiogenesis in an ischemic hindlimb model. *Journal of Molecular and Cellular Cardiology, 48*, 680–693.
59. Joshi, S., Singh, A., Zulcic, M., & Durden, D. (2014). A macrophage-dominant PI3K isoform controls hypoxia-induced HIF1α and HIF2α stability and tumor growth, angiogenesis, and metastasis. *Molecular Cancer Research: MCR, 12,* 1520–1531.
60. Chen, Y., Tian, L., Wan, S., Xie, Y., Chen, X., Ji, X., et al. (2016). MicroRNA-17-92 cluster regulates pancreatic beta-cell proliferation and adaptation. *Molecular and Cellular Endocrinology, 437,* 213–223.